Materials Science Forum
ISSN: 1662-9752, Vol. 1004, pp 689-697
doi:10.4028/www.scientific.net/MSF.1004.689

Submitted: 2019-09-18
Revised: 2019-11-15
Accepted: 2019-11-22
Online: 2020-07-28

Intentional and Unintentional Channeling during Implantation of p-Dopants in 4H-SiC

M.K. Linnarsson[1,a*], A. Hallén[2,b], and L. Vines[3,c]

[1]Materials and Nano-Physics, KTH Royal Institute of Technology, Electrum 229, SE-164 40 Kista, Sweden

[2]School of EECS, KTH Royal Institute of Technology, Electrum 229, SE-164 40 Kista, Sweden

[3]Physics Department/Center for Materials Science and Nanotechnology, University of Oslo, P.O. Box 1048 Blindern, N-0316 Oslo, Norway

[a]marga@kth.se, [b]ahallen@kth.se, [c]lasse.vines@uio.no

Keywords: Channeling implantation, p-dopants, SIMS, damage, electronic stopping, Monte Carlo simulations, binary collision approximation

Abstract. Channeling phenomena during ion implantation have been studied for 50 keV ^{11}B, 100 keV ^{27}Al and 240 keV ^{71}Ga in 4H-SiC by secondary ion mass spectrometry and medium energy ion backscattering. The same projected range is expected for the used energies while the channeling tails are shown to be substantially different, for example, channeled ^{71}Ga ions may travel 5 times as deep as ^{11}B. Ion implantation has been performed both at room temperature (RT) and at 400 °C, where channeling effects are reduced for the 400 °C implantation compared to that of the RT due to thermal vibrations of lattice atoms. The temperature effect is pronounced for ^{71}Ga but nearly negligible for ^{11}B at the used energies. The channeling phenomena are explained by three-dimensional Monte Carlo simulations. For standard implantations, i.e. 4° off the c-direction, it is found that a direction in-between the [000-1] and the <11-2-3> crystal channels, results in deep channeling tails where the implanted ions follow the [000-1] and the <11-2-3> directions.

Introduction

Ion implantation is a common process in device manufacturing for introduction of dopants. Typically, ion implantation in 4H-SiC is performed using the standard miscut of the wafer, 4° off-axis from the [0001] towards the [11-20] direction, as a "random", or non-channeling direction. This is expected to result in an almost Gaussian shaped depth profile. If the implantation is instead performed along a major crystal axis, the ions will follow the crystal direction substantially deeper into the crystal [1-3] and the concentration versus depth profile will have a broader distribution [4-6]. However, even for implantations 4° off from the [000-1] direction, some ions will be steered into crystal channels and these ions will contribute to a deep tail in the dopant distribution [7]. In SiC, the channeled ions may come to rest significantly deeper than the projected range of an amorphous target [4-9]. The degree of channeling varies with atomic number of implanted ions as well as the energies used. Channeling effects are also known to decrease with increasing temperature, because of lattice vibrations, and for higher fluence, where lattice damage disturbs the ordered channels. [5,6,10]. Furthermore, the depth distribution may be altered by the presence of a surface contamination and/or native oxide (SiO_2), which may further reduce the channeling [11].

For SiC devices, a few attempts have been made to utilize the channeling effects to create deeper and more elongated profiles [12]. However, most implantations are performed at elevated temperature, where the channeled profiles are different from those achieved at RT due to a decrease in penetration depth of channeled ions caused by lattice vibrations [4,5]. On the other hand, at elevated temperatures the damage annealing increases, resulting in a trade-off for the channeling effect between increasing temperature and damage build-up.

To predict and investigate channeling phenomena in crystalline 4H-SiC during ion implantations several Monte Carlo Codes are used [13-17]. These codes are usually based on the binary collision approximation (MC-BCA) and use the algorithms that stem from the so-called MARLOWE code

[13,14]. In this study, we have investigated intentional and unintentional channeling during implantation of p-type dopants into 4H-SiC (0001). Implantations have been performed both at room temperature (RT) and at 400 °C. MC-BCA simulations have been used to support, explain and predict experimental results for various incident ions at different temperatures.

Experimental

A 100 keV proton beam has been used to acquire the blocking pattern from backscattered protons. From such "channel maps" the crystal orientation relative to the incoming beam can be deduced. For this, a medium ion energy spectrometer with a high-precision, six-axis goniometer and a large area position sensitive detector has been used. In addition, blocking patterns of backscattered ions have been recorded for out-going 40 keV protons and 40 keV B-ions.

After alignment of the sample, the ion source was reconfigured and ion implantations of 50 keV boron, 100 keV aluminum or 240 keV gallium where performed at angles between [000-1] (0°) and <11-2-3> (17°), i.e, the sample was rotated from the <0001> towards the <11-20> direction. The used energies have been chosen to give the three ions the same projected range according to SRIM for an amorphous target using the atomic density of crystalline 4H-SiC [20]. Doses in the range of 3.7×10^{13} – 1.3×10^{15} cm^{-2} have been used at RT and 400 °C. The ion implantations have been performed in different areas of 5×11 mm^2 4H-SiC samples cut from a wafer with a 10 µm thick, n-type epitaxial layer (5×10^{15} N/cm^3) purchased from Ascatron AB.

Analysis of the obtained depth distribution of ^{11}B, ^{27}Al and ^{71}Ga were performed via secondary ion mass spectrometry (SIMS) in a Cameca IMS7f micro analyzer. A primary sputtering beam of 10 keV $^{32}(O_2)^+$ ions was applied and positive secondary ions were detected. High mass resolution was applied for ^{71}Ga detection. In order to minimize the effect of sample charging, gold coating was used when needed.

Simulations

Simulations were performed using the Monte Carlo binary collision approximation (MC-BCA) code SIIMPL [17] to predict implantation profiles, recognize preferential channeling directions in the crystal, and to understand the complicated trade-off between temperature and damage build-up for the channeling. In this code, the universal potential of Ziegler, Biersack and Littmark (ZBL) [20] is used and the scattering integral is solved by the "Magic- Formula" [21]. The lower electronic stopping in channels has been accounted for by modifying the random electronic loss, S_e, by the expression $S_e A\exp(-sp/a_u)$, where s, p, a_u and A are: a fitting constant, the impact parameter, the universal screening length and a normalization constant, respectively. In this report, s is dependent on the incident ion. The random electronic stopping, S_e, is expressed as kE^b where k and b are constants determined in ref. 22. Thermal vibrations have been included in the model according to the mean-square displacement of carbon and silicon atoms at RT, 0.057 and 0.051 Å, respectively [23], while at 400 °C the mean-square displacements have been determined by fitting simulations with experimental data for different ions and doses. Dynamic annealing of damage has been included in the model [10]. The native self-oxide and adhesive contaminations at the surface are approximated by an amorphous top-layer of 8 and 4 Å at RT and 400 °C, respectively

Results and Discussion

In Fig. 1 b - d., three polar maps of the blocking patterns are shown for 4H-SiC measured by backscattering with outgoing energies of b) 40 keV protons, c) 100 keV protons and d) 40 keV boron ions while the used geometry is sketched in a). The intensity is given by colors where darker blue represents a lower number of backscattered ions and arises from high-symmetry axes and planes. The six-fold symmetry of 4H-SiC is seen from the {11-20} planes intersecting each other along the [0001] direction. The off angles of 5°, 10°, 15° and 17° from the [0001] direction, used as the 0° direction in the polar map are indicated by white dotted lines. At 17° off from [0001], in the {1-100} plane, a

large crystal channel, the <11-23> direction, is clearly visible as a dark blue spot. Between 8° and 9° off from [0001], in the {1-100} plane, smaller blue spots are visible, corresponding to <11-26>. A blocking pattern is an (inverted) image of axial and planar channels, which is specific for different ions and energies. Therefore, the width of the dark blue lines and the sizes of darker dots, show angles at which the probability for channeling of impinging ions will be high. If the planes and axes are narrow in the blocking pattern the critical angle for an ion to be channeled is small and only directions very close to the axes and planes will result in channeling. The decrease of critical angle with increasing energy is illustrated by two polar maps recorded for 40 keV and 100 keV protons (Fig. 1b and Fig. 1c), where the higher energy results in significantly sharper features. For 40 keV boron ions (Fig. 1d), having a larger mass than protons, the {11-20} planes and the [0001] direction are large and the critical angle for channeling into [000-1] is around 4°. This means that using the standard 4° miscut wafers for 40 keV boron implantations with incidence angle normal to the wafer surface results in an implantation profile with a deep B tail due to channeled ions. In addition to these directly channeled ions, there is always a probability that an ion outside the critical angle for channeling after a few collisions may be steered into major crystal planes and/or directions. This means that it will not be possible to avoid deep tails in crystalline SiC during ion implantation, only to minimize the contribution from channeling effects in the desired depth profile.

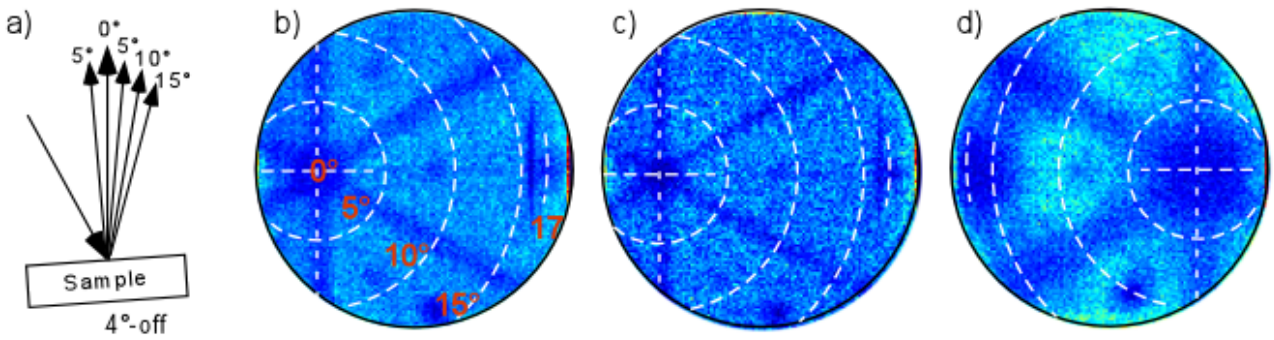

Figure 1. The geometry is sketched in a), while blocking pattern are shown for 4H-SiC shown for backscattered b) 40 keV and c)100 keV protons and d) 40 keV boron ions as polar maps. Backscattered angles of 5°, 10°, 15° and 17° from 0°, the [0001] direction, are included in the polar map as white dotted lines.

The depth distributions of three 50 keV B implants measured by SIMS are displayed in Fig. 2. These implantations are performed at RT using three different impact angles, 0°, 5° and 17° off from the [000-1] direction towards the <11-20> direction. In addition, a depth profile calculated by the SRIM code has been included [20]. As expected from the polar map (Fig. 1d), completely different profiles are obtained as the direction of the implantation is changed. If the ion beam is aligned parallel to the [000-1] direction, a broad distribution is obtained where the concentration peaks at a significantly larger depth than the expected projected range in an amorphous target (0.11 µm) calculated with the same atomic density as a crystalline sample. As the impinging ion beam is 5° off from the [000-1] direction towards the <11-20> direction, the peak maximum moves closer to the surface and approaches the projected range for an amorphous target. However, a tail with lower concentration is present, which extends as deep as the tails in the implantation performed directly into the [000-1] direction. For the 5° off sample, the boron concentration in the tail between 0.2 and 0.5 µm indicates that about 1% of the ions have been steered into a crystal channel. As a result, the ions move deep into the sample.

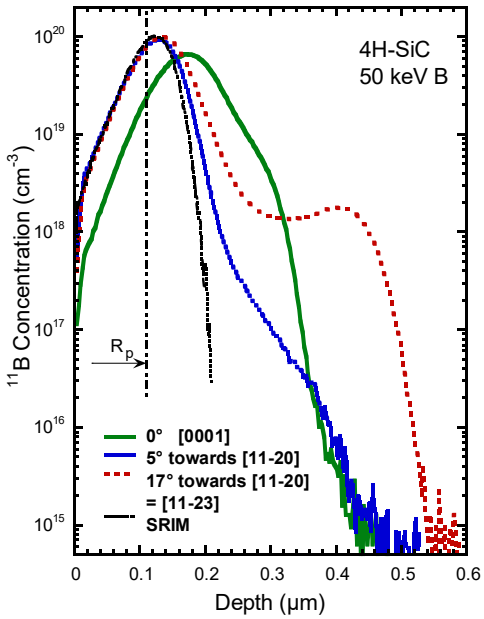

Figure 2. SIMS measurements from three boron implants in 4H-SiC, where the ion implantation has been performed at angles of 0°, 5° and 17° off from the [000-1] towards the <11-20> direction. A depth profile with R_p=0.11μm, simulated by the SRIM code, is also included.

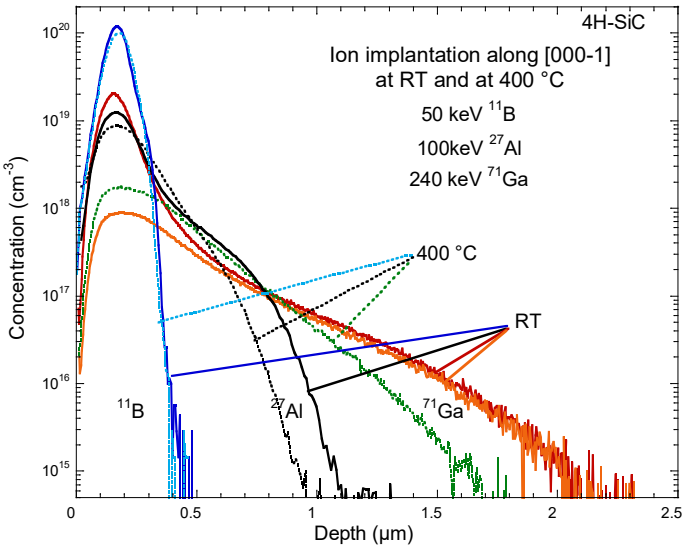

Figure 3. Seven SIMS profiles showing the depth distribution of 50 keV ^{11}B, 100 keV ^{27}Al and 240 keV ^{71}Ga in 4H-SiC after ion implantation aligned along the [000-1] direction. Doses between 3.7×10^{13} and 1.2×10^{15} cm^{-2} have been used. The implant temperature was RT or 400 °C. For ^{71}Ga, two RT profiles with different doses are displayed.

When the impinging beam is at 17° off from the [000-1] direction towards the <11-20>, i.e. with the beam parallel to <11-2-3>, the concentration profile displays two maxima. One major peak around 0.13 μm and a second one at about 0.42 μm. The concentration at the two peaks is dose dependent, since the damage increases for higher doses and this accumulated damage will effectively block further channeling.

From SRIM calculation [20], it is expected that the ion implantation of 50 keV ^{11}B, 100 keV ^{27}Al or ^{71}Ga in 4H-SiC should result in similar depth distributions of dopants. However, this is clearly not the case for crystalline 4H-SiC, as seen in Fig. 3, showing SIMS measurements of dopants concentration versus depth for seven implantations along the [000-1] direction. The maximum concentrations are at similar depth for 50 keV ^{11}B, 100 keV ^{27}Al and 240 keV ^{71}Ga, while the channeling tails are very different. Four of the samples have been implanted at RT and three at 400 °C. The doses used are chosen above the dose where channeling reaches a saturation due to dechanneling from damage. Hence, additional ions distribute around the random peak. At high doses, the implantation induced damage plays a predominant role and the channeling will cease due to the large number of interstitial atoms blocking the channels. This effect is shown for ^{71}Ga implanted at RT with two different doses, 3.7×10^{13} and 3.0×10^{14} cm^{-2}; as the dose increases the concentration in the peak increases while the tail remains the same. Instead, the dopants builds-up around the projected range for a random implantation and the RT curves have kinks, or knees, on the deeper side of the profile. As the mass and energy increase, from ^{11}B to ^{71}Ga, the concentrations at the knees decrease and the penetration depths increase. The concentration level of these knees are for ^{11}B, ^{27}Al and ^{71}Ga about 1×10^{19}, 1×10^{18} and 1×10^{17} cm^{-3}, respectively and the penetration depth increases from 0.5 μm for ^{11}B to 2.2 μm ^{71}Ga ions. These differences for ^{11}B, ^{27}Al and ^{71}Ga ions in 4H-SiC may be understood by the absence of energy loss from nuclear collisions for channeled ions, where the channeled ^{71}Ga ions will travel closer to the center of the channel compared to channeled ^{27}Al and ^{11}B ions [15].

For ^{11}B, only a minor difference is present between implantations made at RT and 400 °C, while ^{27}Al and ^{71}Ga channeled ions travels much deeper and exhibits a significant difference between RT

and 400 °C. At elevated temperatures, as lattice vibration increases, the available open space in a channel decrease. If the channel "width" is large compared to the lattice vibrations, thermal vibrations will only result in a minor reduction of the penetration depth, as in the case of ^{11}B. On the other hand, ^{27}Al and ^{71}Ga reveal that if thermal vibrations of atoms are of the same order as the "width", the depth distribution will be strongly effected, as shown in Fig. 3. Note also that, the tail is deeper for ^{71}Ga compared to ^{27}Al and the influence from lattice vibrations are larger, indicating that the channels are wider for ^{27}Al compared to ^{71}Ga. For the 400 °C implantations the knees in the profiles are at a slightly higher concentrations compared to RT, but the tail is not so extended. This is due to two counteracting processes. Firstly, at elevated temperatures an increasing number of ions may be dechanneled, caused by increasing lattice vibrations resulting in a shallower profile, as displayed for ^{27}Al and ^{71}Ga. Secondly, a larger fraction of the ion induced damage will anneal due to dynamic annealing, leading to a lower degree of dechanneling and a higher concentration at the knee.

To investigate the origin of the long tails during ion implantation into 4H-SiC, three dimensional (3D) MC-BCA simulations have been performed. Figure 4 presents 3D-images of the simulation results for 50 keV $^{11}B^+$ (a), 100 keV $^{27}Al^+$ (b) and 240 keV $^{71}Ga^+$-ions (c). Also included are 2D-cross sections and 1D-depth profiles that have been extracted from the 3D-simulations. In the simulations, the ions are impinging perpendicular to the sample surface, which has a 4° miscut, i.e., a typical configuration used for ion implantation of 4H-SiC. The original ion direction is indicated in Fig. 4 by a red line for the 3D-images, or a dotted red line for the 2D-images. In the simulations 1.5×10^7 ions have been simulated, thermal vibrations for RT have been used and, to include the build-up of damage, a dose of 5×10^{14} cm^{-2} have been utilized. A small impact area of 1×1 nm^2 has been used to readily identify the preferred crystallographic directions for channeling. It should be pointed out that a dose of 5×10^{14} cm^{-2} corresponds to 5 ions per nm^2 and the simulations only show the probability to find an ion at a particular position.

In Fig. 4, the major part of the dopants is enclosed in a dense drop-shaped volume close to the surface. The extension of this drop is due to lateral and range straggling, as expected for an amorphous target. Below this drop-shaped volume, seven main channeling directions are present, the [000-1] direction and the six members of the <11-2-3> family. For ^{11}B, ^{27}Al and ^{71}Ga, the channeling tails with the highest concentration is along the [000-1] directions, while the deepest tails are found along the six <11-2-3> directions. From a top view image (not shown), planar channeling in the {11-20} planes is also visible. In addition, a few ions may find their way to other symmetry directions and, for instance, the probability for scattering into the wide open <11-20> direction is not negligible [24].

To further highlight the [000-1] and the <11-23> directions, 2D-cross sections are shown in the {-1100} plane where only 6 nm thick slices are displayed to exclude all scattering directions not in the {-1100} plane. This is done to simplify identification of channel directions and should not be confused by the 6-fold symmetry. In these cross sections, the vertical channels are the [000-1] directions and the two lines, 17° off, are two members of the <11-23> family. For the ions used, the main part of the channelled ions is steered into [000-1] directions, but there is also a significant probability for ions to be channeled along <11-2-3> directions. For ^{11}B, the channeling tails are five times as deep as the projected range, while for ^{71}Ga the channeled ions reach about 20 times as deep.

Comparing the 1D concentration profiles with the 2D and 3D images, the relative contribution in the 1D depth distribution from [000-1] and <11-2-3> directions can be seen. For example, for ^{27}Al, two knees are seen in the concentration curve (named 1 and 2 and indicated by arrows in the figure). In the first part of the tail (0.5-1μm) the main contribution is from the [000-1] direction and for the second part of the tail the contribution relates to <11-2-3> directions (1-2.5 μm). Going from 1 to 2 the concentration decreases 100 times and the concentrations at 2 are found to be ~ 1×10^{16}, 1×10^{15} and 1×10^{14} cm^{-3} for ^{11}B, ^{27}Al and ^{71}Ga, respectively. However, if the sample is rotated from 4° off angle towards <11-20>, the contribution from the [000-1] direction decreases, while channeling along <11-2-3> directions will become more important [7].

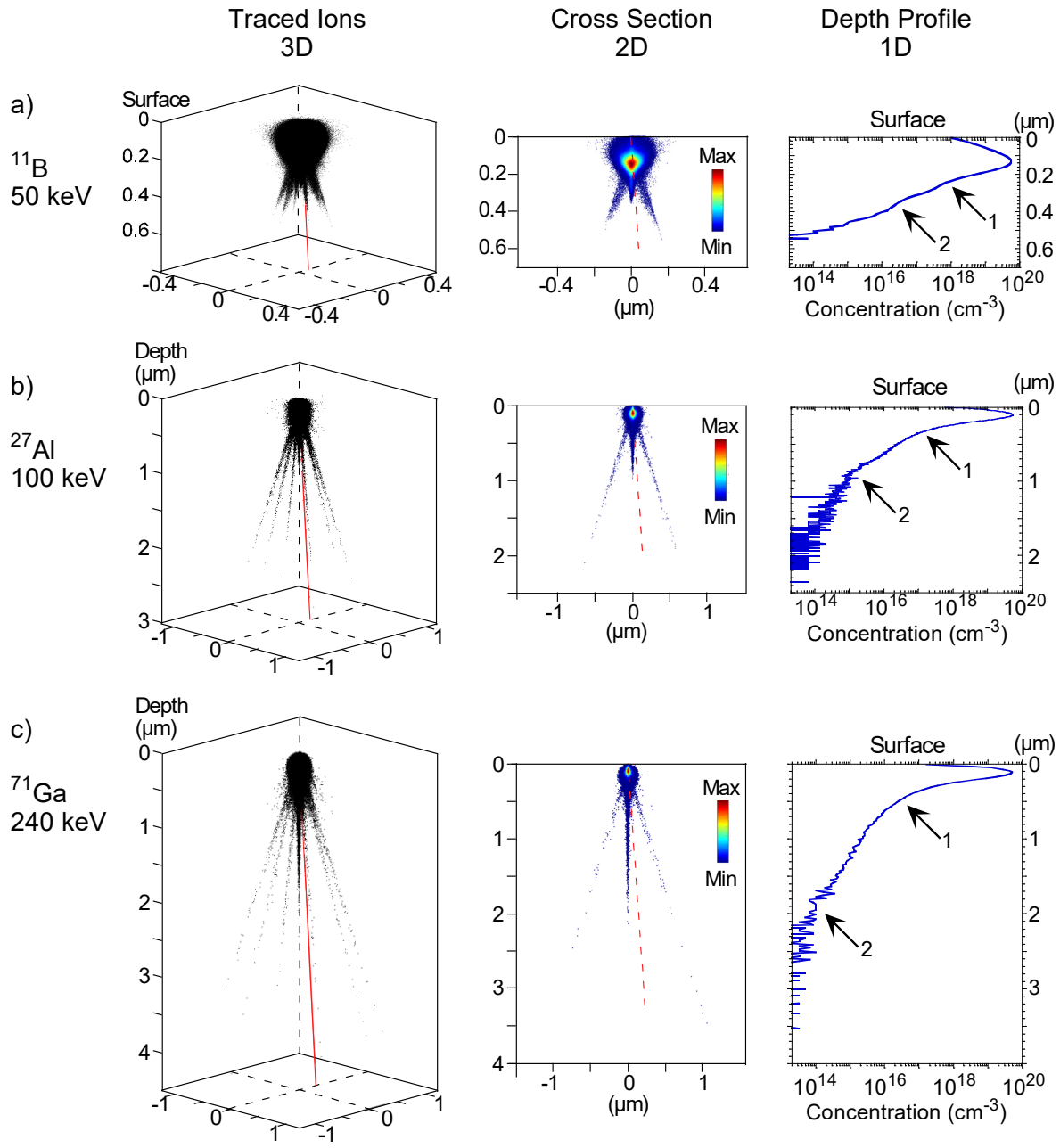

Figure 4. To the left are three 3D simulations displaying the probability to find an implanted ion at a certain position in a 4H-SiC lattice after ion implantation with 50 keV ^{11}B (a), 100 keV ^{27}Al (b) and 240 keV ^{71}Ga (c) ions. A dose of 1.5×10^{7} ions has been traced and an impact area of 1×1 nm^2 and 4° off angle have been employed. An ion dose of 5×10^{14} cm^{-2} has been utilized to include the build-up of damage. In the middle column, 2D cross sections in the {1-100} plane, 6 nm thick slices that have been extracted from the 3D data. To the right are concentration versus depth profiles,1D distribution calculated from the 3D data The MC-BCA code SIIMPL has been used for the simulations [17].

Three-dimensional simulations have also been carried out for 100 keV ^{27}Al-ions using a larger impact area of 1×1 μm^2, an area more relevant to device dimensions. These ions are implanted perpendicular to the sample surface of wafers with a 4° miscut. A number of 2×10^{7} ions have been tracked and a dose of 4×10^{13} cm^{-2} has been used. The 3D data from the simulations are displayed in Fig. 5 as, a) 2D- top view and b) cross section in the {1-100} plane on a linear scale as well as c) 1D concentration versus depth profile on a log scale. In the top view, Fig. 5a, all tracked ions are included as black dots and the impact area is indicated by a red square. A yellow line shows the position of the cross section, which is a 10 nm thick slice that has been cut out and displayed in Fig. 5b. The impact

area is evidently smaller than the extension of the distribution and part of this broadening is expected from lateral straggling. In addition, there is a minor probability to find channeled ions far away from the square.

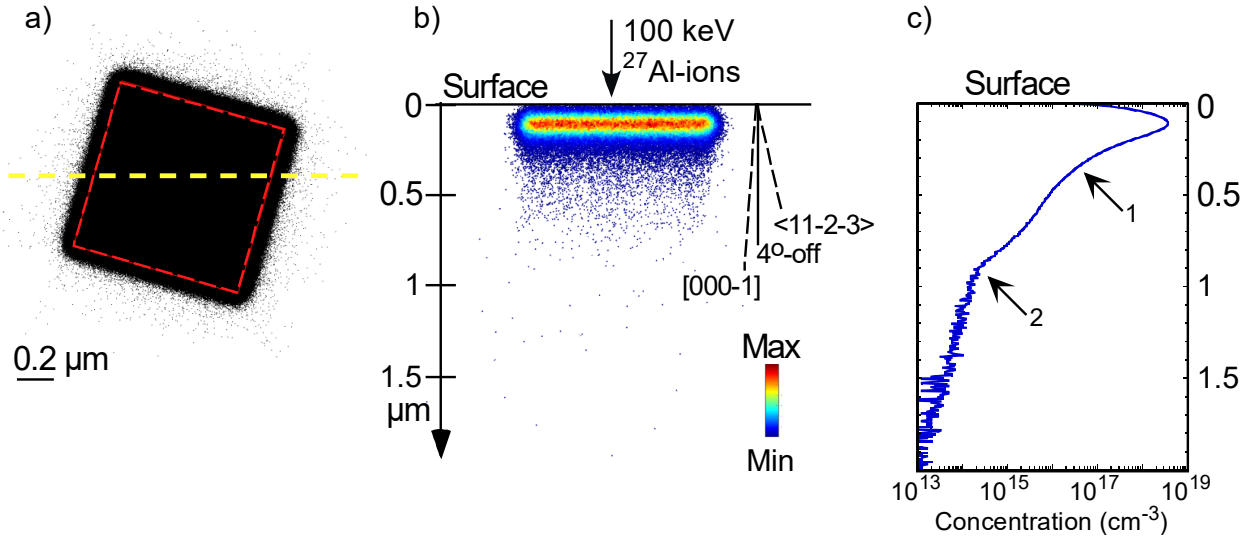

Figure 5. 3D-simulated data for RT implantation of 100 keV ^{27}Al in 4H-SiC using the 4° miscut. 2×10^7 ions have been simulated, an impact area of 1×1 µm^2 and a dose of 4×10^{13} cm^{-2} has been used. a) shows a top-view where the impact area is indicated by a red dashed line and the used position of the cross section in b) is indicated by a yellow dashed line. In b) the simulated data is displayed as a 2D cross section in a 10 nm thick slice in the {-1100} plane. All simulated ^{27}Al-ions are included as black dots for the top-view, while the concentration is represented by a color scale in the cross section. In c) the 1D-concentration versus depth is displayed where arrows 1 and 2 indicate knees in the tail distribution.

In Fig. 5b, the cross section shows that in addition to the main peak around the projected range, there is an extended contribution from channelled ions. To the right in Fig. 5b, crystal directions have been included as to guide the eye. Close to the surface, within 0-0.4 µm, the outer edges of the implanted distribution are rounded. Further down, around 0.4-0.9 µm, a broad band is seen where the outer edges are parallel to [000-1]. In addition, there is a small probability to find the ions much deeper and far away from the [000-1] direction. This is in agreement with simulations using a small impact area, 1×1 nm^2, while simulation results from a large impact area can be viewed as the overlap of parallel distributions. However, it is challenging to identify the <11-2-3> directions, 17° off from [000-1] in Fig. 5b. However, in Fig.5c, a similar concentration curve, with two knees (1 and 2) are obtained as for the small area implantation. Hence, the main contribution to the tails starting at 1 and 2, are expected to originates from the [000-1] and <11-23> directions, respectively, i.e., from Fig. 5c it is clearly seen that the contribution from channelled ions in these two directions needs to be taken into account for device implantations.

Summary

In this contribution, we have presented experimental data and MC-BCA simulations for intentional and unintentional channeling of 50 keV ^{11}B$^+$, 100 keV ^{27}Al$^+$ and ^{71}Ga$^+$ ions in 4H-SiC at RT and 400 °C. Preferential planes and directions for ions are visualized by blocking maps using medium energy ion scattering. For ^{11}B$^+$ ions, the {11-20} plane as well as [0001], the <11-23> and <11-26> directions can be recognized. These crystal planes and channels can contribute to ion channeling. Data from SIMS show that both concentration and depth distribution depends on the used ion, where the depth of the deepest channeled ions increases drastically for the acceptor dopants, going from ^{11}B via ^{27}Al to ^{71}Ga, while the concentration decreases.

The probability for channeling during implantations at 400 °C relative to RT is similar for ^{11}B$^+$ ions, while the channeling depth is drastically reduced for ^{27}Al$^+$ ions and even more for ^{71}Ga$^+$ ions

when raising the temperature. These effects are due to larger effective channels leading to less interaction with the lattice atoms. Hence, the effect on the channel cross sections from thermal vibrations is small for $^{11}B^+$ ions compared to $^{27}Al^+$ and $^{71}Ga^+$ ions, where the effective channel cross sections are relatively narrow.

From 3D MC-BCA simulations the most important channels can be identified. In addition, the expected concentration versus depth profiles are predicted for implantations into 4H-SiC(0001) samples using the 4° miscut angle. The simulations show that both channeling along the [000-1] direction and the <11-2-3> directions are present, but the contribution to the total depth concentration profile from [000-1] direction results in higher concentrations while <11-2-3> gives deeper tails. By rotating the sample, the relative contribution to channeling tails from the [000-1] direction and the <11-2-3> directions can be changed but channeling effects cannot be avoided.

Acknowledgment

Financial support by the Swedish Research Council (VR E0510501), the Ion Technology Centre, ITC, in Sweden via VR-RFI (contract #2017-00646_9) and the Swedish Foundation for Strategic Research (SSF, contract RIF14-0053) and the Research Council of Norway through the research project FUNDAMeNT (no. 251131), and the Norwegian Micro and Nano-Fabrication Facility NorFab (no. 245963) are gratefully acknowledged.

References

[1] D.S. Gemmell, Rev. Mod. Phys. 46 (1974) 129.

[2] K. Nordlund, F. Djurabekova and G. Hobler, Phys. Rev. B94 (2016) 214109.

[3] A. Vantomme, Nucl. Instr. Meth. B371 (2016) 12.

[4] A. Hallén, M.K. Linnarsson and L. Vines, Mater. Sc. Forum, 963 (2019) 375.

[5] M.K. Linnarsson, A. Hallén, L. Vines and B.G. Svensson, Mater. Sc. Forum, 963 (2019) 382.

[6] K. Mochizuki, R. Kosugi, Y. Yonezawa and H. Okumura, Jpn. J. Appl. Phys 58 (2019) 050905.

[7] M.K. Linnarsson, A. Hallén and L. Vines, Semicond. Sci. Technol., (2019) accepted.

[8] P. Pichler, T. Sledziewski, V. Häublein, A.J. Bauer and T. Erlbacher, Mater. Sc. Forum, 963 (2019) 386.

[9] J. Wong-Leung, M.S. Janson and B.G. Svensson, J. Appl. Phys. 93 (2003) 8914.

[10] M.S. Janson, A. Hallén, P. Godignon, A.Yu. Kuzneetsov, M.K. Linnarsson, E. Morvan and B.G. Svensson, Mat. Sci. Forum 338-342 (2000) 889.

[11] A.E. Michel, R.H. Kasti, S.R. Mader, B.J. Masters and J. A. Gardner, Appl. Phys. Lett. 44 (1984) 404.

[12] Suvorov A V, Pala V, U.S. Patent 0069083 A1(2018).

[13] M. Posselt, B. Schmidt, T. Feudel and N. Strecker, Material Science and Engineering B71, (2000) 128.

[14] G. Lulli, E. Albertazzi, M. Bianconi, R. Nipoti, M. Cervera, A. Carnera, and C. Celini, J. Appl. Phys. 82 (1997) 5958.

[15] G. Hobler, Nucl. Instr. Meth. B96 (1995) 155.

[16] E. Morvan, P. Godignon, J. Montserrat, J. Fernández, D. Flores, J. Millán and J.P. Chante, Mat. Sci. Eng. B46 (1997) 218.

[17] M.S. Janson, PhD Thesis, KTH-Royal Institite of Technology, Department of Microelectronics and Information Technology, Materials and Semiconductor Physics Laboratory, Sweden, (2003) ISSN0284-0545.

[18] M.T. Robinson O.S. and Oen, Phys. Rev. 132 (1963) 2385.

[19] M. T. Robinson and I.M. Torrens, Phys. Rev. B9 (1974) 5008.

[20] J.F. Ziegler, J.P. Biersack, and Y. Litmark, The stopping and ranges of ions in solids, Pergamon Press, 1985.

[21] J.P. Biersack and L. Haggmark, Nucl. Instr. Meth. 174 (1980) 257.

[22] M.S. Janson, M.K. Linnarsson, A. Hallén and B.G. Svensson, J. Appl. Phys. 96 (2004) 164.

[23] A. Zywietz, K. Karch and F. Bechstedt, Phys. Rev. B54 (1996) 1791.

[24] G. Lulli, IEEE, Trans. Electron Devices 58 (2011) 190.